# Higher-dimensional Hofstadter butterfly on the Penrose lattice

Rasoul Ghadimi [1,2,3] Takanori Sugimoto [4,5] and Takami Tohyama [6]

[1] *Center for Correlated Electron Systems, Institute for Basic Science (IBS), Seoul 08826, Korea*
[2] *Department of Physics and Astronomy, Seoul National University, Seoul 08826, Korea*
[3] *Center for Theoretical Physics (CTP), Seoul National University, Seoul 08826, Korea*
[4] *Center for Quantum Information and Quantum Biology, Osaka University, Osaka 560-0043, Japan*
[5] *Advanced Science Research Center, Japan Atomic Energy Agency, Tokai, Ibaraki 319-1195, Japan*
[6] *Department of Applied Physics, Tokyo University of Science, Tokyo 125-8585, Japan*

It is now possible to use quasicrystals to search for novel topological phenomena enhanced by their peculiar structure characterized by an irrational number and high-dimensional primitive vectors. Here, we extend the concept of a topological insulator with an emerging staggered local magnetic flux (i.e., without external fields), similar to Haldane's honeycomb model, to the Penrose lattice as a quasicrystal. The Penrose lattice consists of two different tiles, where the ratio of the numbers of tiles corresponds to an irrational number. Contrary to periodic lattices, the periodicity of the energy spectrum with respect to the magnetic flux no longer exists, reflecting the irrational number in the Penrose lattice. Calculating the Bott index as a topological invariant, we find topological phases appearing in a fractal energy spectrum similar to the Hofstadter butterfly. More intriguingly, by folding the one-dimensional aperiodic magnetic flux into a two-dimensional periodic flux space, the fractal structure of the energy spectrum is extended to a higher dimension, whose section corresponds to the Hofstadter butterfly.

The essential characteristics of quasicrystalline physical properties have continuously been sought and discussed since the astonishing discovery of quasicrystals [1], because of their distinct characteristics; higher-order (five-, eight-, or tenfold) rotational symmetry, an irrational ratio of the numbers of different local structures, fractality in their global structure, and higher-dimensional primitive vectors, instead of translational symmetry [1–3]. The first investigations on single-particle electronic properties have been performed more than three decades ago [4–13], resulting in several discoveries of quantum properties in quasicrystals, e.g., (critical or confined) zero-energy eigenstates [9–13], and (multi)fractal structures in an energy spectrum [6,14–16]. In parallel, the thermodynamical properties in quasicrystals have also retained much interest, because of a specific lattice degree of freedom, the so-called phason, corresponding to a hidden degree of freedom related to the higher dimension [14,17,18]. Furthermore, recent experimental discoveries of quasicrystalline ferromagnetism, superconductivity, and quantum criticality [19–22], and successful realizations of aperiodic optical lattices [16,23] and topological photonic quasicrystals [24–26] have spurred theoretical investigations of exotic physical properties in quasicrystals. In addition, recent attempts to discover novel phases of matter have been focused on the topological phases in quasicrystals: topological insulators [27–37], topological superconductors [38–41], higher-order topological phases [36,42], and hidden topologies in non-Hermitian systems [43,44].

Despite the recent progress in the topological phases of quasicrystals, the essential properties in quasicrystals have still not been completely clarified so far. To extract an essential property common in quasicrystals, we focus on the irrational number characterizing the quasicrystalline structure. In quasicrystals, the irrational number corresponds to the ratio of the numbers of two different tiles and the ratio of surfaces of the tiles, e.g., the golden ratio $(1 + \sqrt{5})/2 (= \tau)$ for the Penrose lattice [see Fig. 1(a)] and the silver ratio $1 + \sqrt{2}$ for the Ammann-Beenker lattice [45,46]. Yet, how do we capture the advent of the irrational number in a physical quantity? Here, we propose a model of a quasicrystalline topological insulator, which is similar to that used by Duncan *et al.* [37] but includes an emerging staggered local magnetic flux (i.e., no external fields). Our proposed model thus corresponds to an extension of Haldane's honeycomb model [47] to quasicrystals.

In Duncan's work [37], they apply a uniform magnetic field and assume local magnetic fluxes proportional to the surfaces of two tiles. Since the ratio of surfaces corresponds to the irrational number in quasicrystals, the ratio of local fluxes becomes the irrational number and breaks the periodicity of the energy spectrum including topological phases with respect to the magnetic flux. However, as mentioned in Ref. [37], the irrational ratio of surfaces is realized even in uniform crystals. On the other hand, the irrational ratio of the numbers of two tiles is undoubtedly unique to quasicrystals. Instead of a uniform magnetic field, if we apply a totally zero staggered magnetic field and impose an equivalent local magnetic flux on the same type of tiles, the ratio of the fluxes can be the irrational number via the ratio of the numbers of tiles. In fact, with the zero external field condition $N_r \phi_r + N_b \phi_b = 0$, the
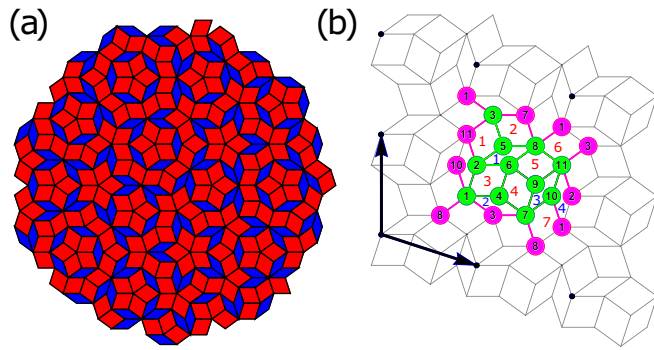
FIG. 1. (a) Penrose lattice constructed by fat (red) and thin (blue) tiles. (b) A $g = 1$ approximant of the Penrose lattice, where the first to 11th green sites are linked by green bonds. Owing to the approximant periodicity, we regard the lattice as a unit cell. The magenta edges linking green to magenta sites denote the bonds bridging between neighboring unit cells, corresponding to a connection of boundaries with a periodic boundary condition. The number colored in red (blue) in each tile counts red (blue) tiles in the unit cell, and the number of red (blue) tiles amounts to 7 (4).

ratio of local fluxes is equivalent to the ratio of the numbers of tiles, i.e., the irrational number, $\phi_r/\phi_b = -N_b/N_r$, where $N_r(N_b)$ and $\phi_r(\phi_b)$ represents the number of red (blue) tiles in Fig. 1(a) and the local flux of them, respectively. Therefore, with a staggered magnetic field, the broken periodicity of an energy spectrum appears only in quasicrystals. Moreover, the aperiodic structure with respect to one of the magnetic fluxes can be folded into a two-dimensional periodic flux space. Adding an energy axis to the two-dimensional flux space, we can see a three-dimensional complicated structure of the energy spectrum, whose vertical section is the so-called Hofstadter butterfly.

In the following, as a case study showing this behavior, we focus on the Penrose lattice, though we have also obtained a qualitatively similar result in an Ammann-Beenker lattice (not shown). The Penrose lattice is a typical example of two-dimensional quasicrystals and is composed of two (fat and thin) rhombuses [see red and blue tiles in Fig. 1(a)]. Although translational symmetry is absent, it has various structural properties, such as fivefold symmetry and self-similarity related to the inflation/deflation rules [45,46]. To demonstrate the numerical results, we use the approximant method to generate a Penrose quasicrystal [10,48]. The quasicrystal approximant has a translationally symmetric structure with a unit cell resembling a local structure of the original quasicrystal [see Fig. 1(b)]. The unit-cell size is increased with increasing the approximant generation $g$, so that the real quasicrystal is obtained with $g \to \infty$ (see Sec. S1 in the Supplemental Material [49]). The numbers of the red and blue tiles in the $g$th generation are $N_r^{(g)} = 3F_{2g+1} + F_{2g}$ and $N_b^{(g)} = F_{2g+1} + 2F_{2g}$, respectively, with the $i$th Fibonacci number $F_i$. According to the inflation rule between the $g$th and $(g-1)$th generations, the number of tiles increases according to $\mathbf{N}_g = \mathbf{F}\mathbf{N}_{g-1}$ with

$$\mathbf{N}_g = \begin{pmatrix} N_r^{(g)} & N_b^{(g)} \end{pmatrix}^T, \quad \mathbf{F} = \begin{pmatrix} 2 & 1 \\ 1 & 1 \end{pmatrix}. \quad (1)$$

Since the eigenvalues of the inflation matrix $\mathbf{F}$ are $\{(1 \pm \sqrt{5})/2\}^2$, in the thermodynamic limit $g \to \infty$, the component of the number's vector $\mathbf{N}_g$ along the eigenvector with the smaller eigenvalue vanishes. The eigenvector for the larger eigenvalue is $(\tau, 1)$ with the golden ratio $\tau$, so that the ratio of the numbers of two tiles converges to the golden ratio, $N_r^{(g)}/N_b^{(g)} \to \tau$ (see Table I). This is a feature peculiar to quasicrystals, while in the periodic lattices consisting of several types of plaquettes, the ratio of the numbers of plaquettes should be rational. We omit the superscript about the generation $(g)$ in the following.

The model Hamiltonian is given by

$$\mathcal{H} = -t \sum_{\langle i,j \rangle} e^{\iota \mathcal{A}_{ij}} c_i^\dagger c_j + \text{H.c.} - \mu \sum_i c_i^\dagger c_i, \quad (2)$$

where $c_i^\dagger$ $(c_i)$ is the creation (annihilation) operator of a spinless fermion at the $i$th vertex on the Penrose lattice, and $\iota$ is the imaginary unit. The chemical potential and the hopping integral are denoted by $\mu$ and $t$, respectively. To introduce a flux in a tile, we use the Peierls phase $\mathcal{A}_{ij}$, corresponding to a line integral of a vector potential on the edge $\langle i, j \rangle$ from the $i$th to $j$th vertices. In addition, to obtain a periodic boundary condition, we use one unit cell of the $g$th Penrose approximant [see Fig. 1(b)].

In the continuum limit, the vector potential $\mathcal{A}(r)$ is related to the magnetic flux $\phi_S$ penetrating the surface $S$ via

$$\phi_S = \oint_{\partial S} \mathcal{A} \cdot dr, \quad (3)$$

where $\partial S$ is the boundary of the surface $S$. In lattice models, we can use an alternative of (3) given by

$$\phi_{(i,j,k,l)} = \mathcal{A}_{ij} + \mathcal{A}_{jk} + \mathcal{A}_{kl} + \mathcal{A}_{li}, \quad (4)$$

where $\phi_{(i,j,k,l)}$ is the magnetic flux passing through a tile constructed by four vertices, $(i, j, k, l)$, numbered counterclockwise. As mentioned above, we assume the same value of flux for each type of tiles, where there are two types of flux $\phi_{(i,j,k,l)} = \phi_r, \phi_b$ for the red and blue tiles in Fig. 1(a), respectively. Moreover, we introduce a constraint on the flux satisfying the totally zero magnetic field $N_r\phi_r = -N_b\phi_b$. In this sense, the two types of flux depend on each other, and are rewritten by

$$\phi_r = 2\pi \frac{n_r}{N_r}, \quad \phi_b = 2\pi \frac{n_b}{N_b}, \quad (5)$$

with a single parameter $n = n_r = -n_b$ as the normalized flux. Note that each magnetic flux has periodicity in the phase space of $[0, 2\pi]$, i.e., the period for $n_r$ $(n_b)$ corresponds to $N_r$ $(N_b)$.

The Peierls phase $\mathcal{A}_{ij}$ is determined as follows. With a fixed normalized flux $n$, we obtain fluxes for two tiles $(\phi_r, \phi_b)$. We computationally assign the local Peierls phase $\mathcal{A}_{ij}$ for edges one by one, satisfying Eq. (4) (see Sec. S2 in the Supplemental Material [49]). Note that the configuration of $\mathcal{A}_{ij}$ is not uniquely assigned, due to the presence of the gauge degree of freedom. However, physical properties should not depend on the gauge transformation: $c_i^\dagger \to e^{\iota\theta_i}c_i^\dagger, c_i \to e^{-\iota\theta_i}c_i$ with $\mathcal{A}_{ij} \to \mathcal{A}_{ij} - (\theta_i - \theta_j)$.

With the configuration of the Peierls phase $\{\mathcal{A}_{ij}\}$, we obtain the energy spectrum by means of numerical diagonalization

TABLE I. The numbers of red and blue tiles, the ratio of them, and the difference from the golden ratio in the Penrose approximants.

| | $g = 1$ | $g = 2$ | $g = 3$ | $g = 4$ | $g = 5$ | $g = 6$ | $g = 7$ |
|---|---|---|---|---|---|---|---|
| $N_r$ | 7 | 18 | 47 | 123 | 322 | 843 | 2207 |
| $N_b$ | 4 | 11 | 29 | 76 | 199 | 521 | 1364 |
| $\frac{N_r/N_b - \tau}{\tau}$ | $O(10^{-1})$ | $O(10^{-2})$ | $O(10^{-3})$ | $O(10^{-4})$ | $O(10^{-5})$ | $O(10^{-6})$ | $O(10^{-7})$ |

of the Hamiltonian (2). Figure 2 shows the energy spectrum in a $g = 7$ Penrose approximant. Since the numbers of tiles $N_r$ and $N_b$ for a given generation $g$ are coprime, the periodicity for the normalized staggered flux $n$ is $N_r \times N_b$, corresponding to $[0, 2\pi N_b]$ for $\phi_r$ and $[0, 2\pi N_r]$ for $\phi_b$. With increasing the generation to the thermodynamic limit, i.e., $N_b \to \infty$, the periodicity of the energy spectrum with respect to the staggered magnetic flux $\phi_r$ or $\phi_b$ no longer remains.

Next, we discuss the topological features by using the Bott index [41,50,51] defined by

$$B_t = \frac{1}{2\pi} \text{Im tr log} \left( V U V^\dagger U^\dagger \right), \qquad (6)$$

with

$$U = P\mathcal{X}P + (I - P), \quad V = P\mathcal{Y}P + (I - P), \qquad (7)$$



$$B_t^\blacktriangle=5 \quad B_t^\blacktriangle=4 \quad B_t^\blacktriangle=3 \quad B_t^\blacktriangle=2 \quad B_t^\blacktriangle=1$$
$$B_t^\blacktriangledown=-5 \quad B_t^\blacktriangledown=-4 \quad B_t^\blacktriangledown=-3 \quad B_t^\blacktriangledown=-2 \quad B_t^\blacktriangledown=-1 \quad B_t^\bullet=0$$
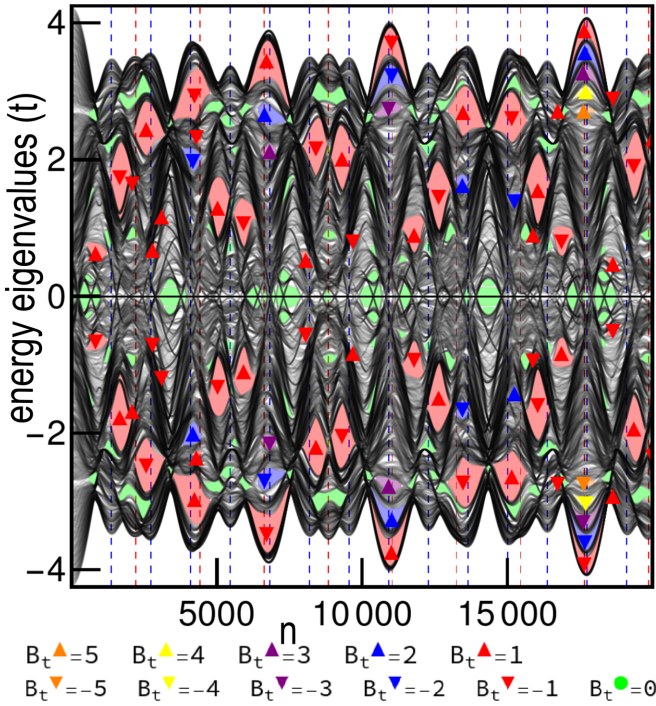
FIG. 2. Energy spectrum of a $g = 7$ Penrose lattice ($N_r = 2207$ and $N_b = 1364$) with anormalized staggered magnetic flux $n$. We set the hopping integral $t = 1$ as an energy unit. The position of the colored symbols denotes the chemical potential $\mu$ (corresponding to the value on the energy axis) and the normalized magnetic flux $n$, and the colored indicators show the Bott index (6) obtained with the parameters $(\mu, n)$. To calculate the Bott index, we choose the chemical potential corresponding to the center of the gap. The gaps are painted with colors representing the Bott index (shown at the bottom of the panel) together with the upper and lower triangles. The vertical dashed lines represent multiples of $N_r = 2207$ (red) and $N_b = 1364$ (blue).

where $P$ is the projection matrix onto lower-lying states than the Fermi level and $I$ is the identity matrix. $\mathcal{X}$ and $\mathcal{Y}$ are the diagonal matrices linking the position to a U(1) phase,

$$\mathcal{X}_{i,j} = \exp \left( 2\pi \iota \frac{x_i - x_{\min}}{x_{\max} - x_{\min}} \right) \delta_{i,j}, \qquad (8)$$

$$\mathcal{Y}_{i,j} = \exp \left( 2\pi \iota \frac{y_i - y_{\min}}{y_{\max} - y_{\min}} \right) \delta_{i,j}, \qquad (9)$$

where $x_{\min}$ and $x_{\max}$ ($y_{\min}$ and $y_{\max}$) are the minimum and maximum values of the $x$ ($y$) component of position, respectively, and $\delta_{i,j}$ is the Kronecker delta. The Bott index gives nonzero integer values in nontrivial topological phases as in the case of other topological invariants. In particular, the Bott index is useful for real-space representations of wave functions, and can be obtained with a periodic boundary condition. Moreover, since the Bott index basically suits a model without time-reversal symmetry, we choose it to calculate the topological number in our model, where time-reversal symmetry is broken due to the staggered magnetic flux. In Fig. 2, we can see some gaps including colored symbols. The colored symbols represent the Bott index at the parameter point of the chemical potential and the normalized flux. We have also checked the appearance of edge modes in the topological phases with the open boundary condition (see Sec. S3 in the Supplemental Material [49]).

As mentioned above, the magnetic flux is unique modulo $2\pi$, i.e., $\phi_r$ and $\phi_b$ can be folded into $[0, 2\pi] \times [0, 2\pi]$, corresponding to a 2-torus. In Fig. 3, we plot the path of flux for
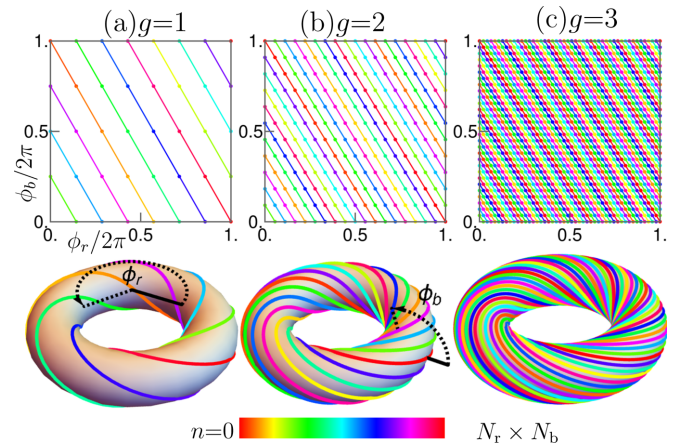


FIG. 3. The path of the possible region of the staggered magnetic fluxes $(\phi_r, \phi_b)$ for $g = 1, 2$, and 3 generations. Since the magnetic flux $\phi_r$ ($\phi_b$) is unique modulo $2\pi$, the parameter space of the two fluxes corresponds to a 2-torus, where the toroidal (poloidal) axis denotes $\phi_r$ ($\phi_b$). With increasing the generation, the path densely covers the whole region of the parameter space, due to approaching the irrational ratio of the fluxes.
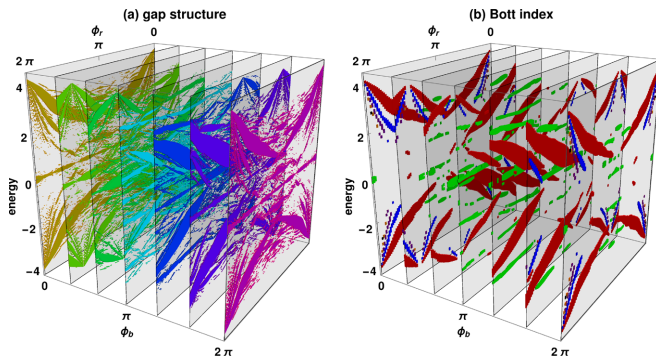
FIG. 4. Three-dimensional Hofstadter butterfly structure. (a) Gap structure and (b) Bott index in the energy spectrum as a function of two independent magnetic fluxes $\phi_r$ and $\phi_b$ in a $g = 7$ Penrose lattice. In (a), only gaps with a size larger than $0.01t$ are shown. In (b), the Bott index is shown for gaps with a size larger than $0.05t$. The colors in (b) are the same as in Fig. 2.

several generations, due to the constraint $\phi_b = -(N_r/N_b)\phi_r$. Note that, even though we can change $\phi_r$ continuously, the folded fluxes in flux parameter space do not occupy a full parameter space for the given generation. However, the possible region of $(\phi_r, \phi_b)$ is expanded with increasing the generation, because of the increase of the smallest common multiple of $N_r$ and $N_b$. This is understood in the following way. For a given $\phi_b$, we can obtain $\phi_r = -N_b/N_r\phi_b - 2\pi N_b/N_r\mathcal{N}$ satisfying the staggered flux distribution, where $\mathcal{N}$ is an arbitrary integer. Consequently, if $N_b$, and $N_r$ do not have any common divisor, then the number of distinguishable $\phi_r$ is obtained by putting $\mathcal{N} = 1, 2, \ldots, N_r$. In the $g \to \infty$ limit, namely in the quasicrystals, the ratio converges to an irrational number (the golden ratio) $N_r/N_b \to \tau$ (see Table I), and $N_r, N_b \to \infty$, so that the possible region of $(\phi_r, \phi_b)$ densely covers the whole space of the 2-torus. Consequently, in the quasiperiodic limit, the magnetic fluxes $\phi_r$ and $\phi_b$ are no longer dependent on each other, and are regarded as two independent parameters. Note that this feature is inherent in the quasicrystals, in contrast to periodic systems such as a kagome lattice [52].

The independence of the magnetic fluxes $\phi_r$ and $\phi_b$ together with an energy axis implies the existence of a three-dimensional structure of the energy spectrum. Figure 4 shows the gap structure in the energy spectrum with two parameters $\phi_r$ and $\phi_b$ (see Sec. S4 in the Supplemental Material for the intersection perpendicular to $\phi_r$, and both intersections together [49]). We can see that the complicated structure, the so-called Hofstadter butterfly, spreads out in three dimensions. By changing the staggered magnetic flux, the system probes this two-dimensional flux phase space in a trajectory shown in Fig. 3. Note that the length of this path in a true quasicrystal limit ($g \to \infty$) is infinite, originating from the golden ratio in the Penrose lattice. Furthermore, we can map the staggered magnetic flux model ($n = n_r = -n_b$) to a nonzero magnetic

flux model ($n' = n'_r = n'_b$), in which the red and blue tiles contain the same flux (see Sec. S5 for the proof [49]).

Finally, we again insist on the similarity and difference between our staggered magnetic flux model and a model with a uniform magnetic field in the quasicrystals proposed in Ref. [37]. The latter model captures an incommensurate behavior of magnetic flux due to the irrational ratio of the surfaces of two tiles, and therefore the phase diagram is an aperiodic function of the magnetic field similar to our model. Folding a resulting energy spectrum as a function in $(\phi_b, \phi_r)$ phase space, one can obtain the same three-dimensional Hofstadter butterfly as our model. However, as mentioned in Ref. [37], one can find the irrational ratio of surfaces of two tiles even in a uniform lattice, e.g., it consists of two rectangles whose surfaces have an irrational ratio. This point is an essential difference between the uniform and staggered fields. In our model, with the staggered field, the aperiodicity of the phase diagram stems from the irrational ratio of the numbers of two tiles. The ratio of the numbers of tiles can be irrational only in quasicrystals, and thus the present feature that we found is unique in quasicrystals.

Artificial magnetic flux distribution has been reported in a chiral phase of an anisotropic XXZ spin model under a perpendicular magnetic field in a kagome lattice [53], where the chirality of the spin configuration produces an effective staggered magnetic flux distribution for coupled conducting electrons [54]. Our preliminary calculations for the anisotropic XXZ model in Ammann-Beenker and Penrose quasicrystals also show the emergence of staggered chiral phases and thus result in a staggered magnetic flux distribution where nontrivial topological phases for coupled conducting electrons appear [55].

In conclusion, we have investigated a tight-binding spinless fermion system on two-dimensional quasicrystals composed of two types of tiles, with an emergent staggered magnetic flux, without external magnetic fields. We found that the energy spectrum and its topological properties are aperiodic as a function of staggered magnetic flux. Furthermore, due to the irrationality of the ratio of the number of the two tiles, two local fluxes are eventually independent in quasicrystals. Consequently, the flux phase space is two dimensional, and increasing staggered magnetic flux probes this flux phase space in a nontrivial way, i.e., the ways never overlap. We found that the energy spectrum in this two-dimensional phase space produces a Hofstadter butterflylike fractal structure, but lives in three dimensions.

[1] D. Shechtman, I. Blech, D. Gratias, and J. W. Cahn, Metallic Phase with Long-Range Orientational Order and No Translational Symmetry, Phys. Rev. Lett. **53**, 1951 (1984).

[2] D. Levine and P. J. Steinhardt, Quasicrystals. I. Definition and structure, Phys. Rev. B **34**, 596 (1986).

[3] J. E. S. Socolar and P. J. Steinhardt, Quasicrystals. II. Unit-cell configurations, Phys. Rev. B **34**, 617 (1986).

[4] M. Arai, T. Tokihiro, T. Fujiwara, and M. Kohmoto, Strictly localized states on a two-dimensional Penrose lattice, Phys. Rev. B **38**, 1621 (1988).

[5] T. Fujiwara, M. Arai, T. Tokihiro, and M. Kohmoto, Localized states and self-similar states of electrons on a two-dimensional Penrose lattice, Phys. Rev. B **37**, 2797 (1988).

[6] T. Tokihiro, T. Fujiwara, and M. Arai, Exact eigenstates on a two-dimensional Penrose lattice and their fractal dimensions, Phys. Rev. B **38**, 5981 (1988).

[7] P. Ma and Y. Liu, Inflation rules, band structure, and localization of electronic states in a two-dimensional Penrose lattice, Phys. Rev. B **39**, 9904 (1989).

[8] T. Fujiwara and T. Yokokawa, Universal Pseudogap at Fermi Energy in Quasicrystals, Phys. Rev. Lett. **66**, 333 (1991).

[9] Y. Liu and P. Ma, Electronic properties of two-dimensional quasicrystals with near-neighbor interactions, Phys. Rev. B **43**, 1378 (1991).

[10] H. Tsunetsugu, T. Fujiwara, K. Ueda, and T. Tokihiro, Electronic properties of the Penrose lattice. I. Energy spectrum and wave functions, Phys. Rev. B **43**, 8879 (1991).

[11] A. Koga and H. Tsunetsugu, Antiferromagnetic order in the Hubbard model on the Penrose lattice, Phys. Rev. B **96**, 214402 (2017).

[12] A. Koga, Superlattice structure in the antiferromagnetically ordered state in the Hubbard model on the Ammann-Beenker tiling, Phys. Rev. B **102**, 115125 (2020).

[13] A. Koga and S. Coates, Ferrimagnetically ordered states in the Hubbard model on the hexagonal golden-mean tiling, Phys. Rev. B **105**, 104410 (2022).

[14] S. Yamamoto and T. Fujiwara, Electronic transport of quasicrystals with random phason strain: The two-dimensional Penrose lattice, Phys. Rev. B **51**, 8841 (1995).

[15] T. Hatakeyama and H. Kamimura, Fractal nature of the electronic structure of a Penrose tiling lattice in a magnetic field, J. Phys. Soc. Jpn. **58**, 260 (1989).

[16] M. A. Bandres, M. C. Rechtsman, and M. Segev, Topological Photonic Quasicrystals: Fractal Topological Spectrum and Protected Transport, Phys. Rev. X **6**, 011016 (2016).

[17] A. Szallas and A. Jagannathan, Phason disorder effects in the Penrose tiling antiferromagnet, Z. Kristallog. **224**, 45 (2009).

[18] For a review, see T. Janssen, G. Chapuis, and M. de Boissieu, *Aperiodic Crystals: From Modulated Phases to Quasicrystals: Structure and Properties* (Oxford University Press, Oxford, U.K., 2018)..

[19] R. Tamura, A. Ishikawa, S. Suzuki, T. Kotajima, Y. Tanaka, T. Seki, N. Shibata, T. Yamada, T. Fujii, C.-W. Wang, M. Avdeev, K. Nawa, D. Okuyama, and T. J. Sato, Experimental observation of long-range magnetic order in icosahedral quasicrystals, J. Am. Chem. Soc. **143**, 19938 (2021).

[20] K. Kamiya, T. Takeuchi, N. Kabeya, N. Wada, T. Ishimasa, A. Ochiai, K. Deguchi, K. Imura, and N. K. Sato, Discovery of superconductivity in quasicrystal, Nat. Commun. **9**, 154 (2018).

[21] K. Deguchi, S. Matsukawa, N. K. Sato, T. Hattori, K. Ishida, H. Takakura, and T. Ishimasa, Quantum critical state in a magnetic quasicrystal, Nat. Mater. **11**, 1013 (2012).

[22] N. K. Sato, T. Ishimasa, K. Deguchi, and K. Imura, Effects of electron correlation and geometrical frustration on magnetism of icosahedral quasicrystals and approximants —an attempt to bridge the gap between quasicrystals and heavy fermions, J. Phys. Soc. Jpn. **91**, 072001 (2022).

[23] L. Guidoni, C. Triché, P. Verkerk, and G. Grynberg, Quasiperiodic Optical Lattices, Phys. Rev. Lett. **79**, 3363 (1997).

[24] Y. E. Kraus, Y. Lahini, Z. Ringel, M. Verbin, and O. Zilberberg, Topological States and Adiabatic Pumping in Quasicrystals, Phys. Rev. Lett. **109**, 106402 (2012).

[25] Y. E. Kraus, Z. Ringel, and O. Zilberberg, Four-Dimensional Quantum Hall Effect in a Two-Dimensional Quasicrystal, Phys. Rev. Lett. **111**, 226401 (2013).

[26] M. Verbin, O. Zilberberg, Y. E. Kraus, Y. Lahini, and Y. Silberberg, Observation of Topological Phase Transitions in Photonic Quasicrystals, Phys. Rev. Lett. **110**, 076403 (2013).

[27] D.-T. Tran, A. Dauphin, N. Goldman, and P. Gaspard, Topological Hofstadter insulators in a two-dimensional quasicrystal, Phys. Rev. B **91**, 085125 (2015).

[28] J.-N. Fuchs and J. Vidal, Hofstadter butterfly of a quasicrystal, Phys. Rev. B **94**, 205437 (2016).

[29] H. Huang and F. Liu, Quantum Spin Hall Effect and Spin Bott Index in a Quasicrystal Lattice, Phys. Rev. Lett. **121**, 126401 (2018).

[30] H. Huang and F. Liu, Theory of spin Bott index for quantum spin Hall states in nonperiodic systems, Phys. Rev. B **98**, 125130 (2018).

[31] H. Huang and F. Liu, Comparison of quantum spin Hall states in quasicrystals and crystals, Phys. Rev. B **100**, 085119 (2019).

[32] J.-N. Fuchs, R. Mosseri, and J. Vidal, Landau levels in quasicrystals, Phys. Rev. B **98**, 165427 (2018).

[33] A.-L. He, L.-R. Ding, Y. Zhou, Y.-F. Wang, and C.-D. Gong, Quasicrystalline Chern insulators, Phys. Rev. B **100**, 214109 (2019).

[34] R. Chen, D.-H. Xu, and B. Zhou, Topological Anderson insulator phase in a quasicrystal lattice, Phys. Rev. B **100**, 115311 (2019).

[35] S. Spurrier and N. R. Cooper, Kane-Mele with a twist: Quasicrystalline higher-order topological insulators with fractional mass kinks, Phys. Rev. Res. **2**, 033071 (2020).

[36] R. Chen, C.-Z. Chen, J.-H. Gao, B. Zhou, and D.-H. Xu, Higher-Order Topological Insulators in Quasicrystals, Phys. Rev. Lett. **124**, 036803 (2020).

[37] C. W. Duncan, S. Manna, and A. E. B. Nielsen, Topological models in rotationally symmetric quasicrystals, Phys. Rev. B **101**, 115413 (2020).

[38] R. Ghadimi, T. Sugimoto, and T. Tohyama, Majorana zero-energy mode and fractal structure in Fibonacci–Kitaev chain, J. Phys. Soc. Jpn. **86**, 114707 (2017).

[39] D. Varjas, A. Lau, K. Pöyhönen, A. R. Akhmerov, D. I. Pikulin, and I. C. Fulga, Topological Phases without Crystalline Counterparts, Phys. Rev. Lett. **123**, 196401 (2019).

[40] Y. Cao, Y. Zhang, Y.-B. Liu, C.-C. Liu, W.-Q. Chen, and F. Yang, Kohn-Luttinger Mechanism Driven Exotic Topological Superconductivity on the Penrose Lattice, Phys. Rev. Lett. **125**, 017002 (2020).

[41] R. Ghadimi, T. Sugimoto, K. Tanaka, and T. Tohyama, Topological superconductivity in quasicrystals, Phys. Rev. B **104**, 144511 (2021).

[42] T. Peng, C.-B. Hua, R. Chen, Z.-R. Liu, D.-H. Xu, and B. Zhou, Higher-order topological anderson insulators in quasicrystals, Phys. Rev. B **104**, 245302 (2021).

[43] S. Longhi, Topological Phase Transition in non-Hermitian Quasicrystals, Phys. Rev. Lett. **122**, 237601 (2019).

[44] S. Weidemann, M. Kremer, S. Longhi, and A. Szameit, Topological triple phase transition in non-Hermitian floquet quasicrystals, Nature (London) **601**, 354 (2022).

[45] M. Senechal, *Quasicrystals and Geometry* (Cambridge University Press, Cambridge, U.K., 1996).

[46] S. Walter and S. Deloudi, Crystallography of Quasicrystals: Concepts, Methods and Structures, *Springer Series in Materials Science* Vol. 126 (Springer, Berlin, 2009).

[47] F. D. M. Haldane, Model for a Quantum Hall Effect without Landau Levels: Condensed-Matter Realization of the "Parity Anomaly", Phys. Rev. Lett. **61**, 2015 (1988).

[48] R. Ghadimi, T. Sugimoto, and T. Tohyama, Mean-field study of the Bose-Hubbard model in the Penrose lattice, Phys. Rev. B **102**, 224201 (2020).

[49] See Supplemental Material at http://link.aps.org/supplemental/10.1103/PhysRevB.106.L201113 for the evolution of the approximant unit cell toward the quasicrystal limit by increasing the generation, details of the calculation for obtaining Peierls phases, visualization of the vector potential for some examples, details of the calculation to obtain the open boundary condition, some examples of topological edge modes in our system, other figures related to the three-dimensional Hofstadter butterfly, and the proof regarding the existence of a map between the staggered magnetic flux model and nonzero magnetic flux model.

[50] I. C. Fulga, D. I. Pikulin, and T. A. Loring, Aperiodic Weak Topological Superconductors, Phys. Rev. Lett. **116**, 257002 (2016).

[51] T. A. Loring, A guide to the Bott index and localizer index, arXiv:1907.11791.

[52] G. Xu, B. Lian, and S.-C. Zhang, Intrinsic Quantum Anomalous Hall Effect in the Kagome Lattice $Cs_2LiMn_3F_{12}$, Phys. Rev. Lett. **115**, 186802 (2015).

[53] H. D. Rosales, F. A. Gomez Albarracín, and P. Pujol, From frustrated magnetism to spontaneous Chern insulators, Phys. Rev. B **99**, 035163 (2019).

[54] K. Ohgushi, S. Murakami, and N. Nagaosa, Spin anisotropy and quantum Hall effect in the kagomé lattice: Chiral spin state based on a ferromagnet, Phys. Rev. B **62**, R6065 (2000).

[55] R. Ghadimi *et al.* (unpublished).